ISSN 0915-633X

NATIONAL INSTITUTE FOR FUSION SCIENCE

Papers Presented at the 6th H-mode Workshop
(Seeon, Germany)

(Received - Oct. 14, 1997)

NIFS-516 Oct. 1997

RESEARCH REPORT
NIFS Series

NAGOYA, JAPAN

Papers presented at the 6th H-mode Workshop (Seeon, Germany)

Abstract

The 6th H-mode workshop was held at Kloster Seeon (Germany) during the period of September 22-24, 1997. Contribution to this workshop is reported. Reports include

1. Role of Nonuniform Superthermal Ions for Internal Transport Barriers (K. Itoh et al.)
2. Electric Field Bifurcation and Transition in the Core Plasma of CHS (A. Fujisawa et al.)
3. Formation and Termination of High Ion Temperature Mode in Heliotron/torsatron Plasmas (K. Ida et al.)
4. Transition to an Enhanced Internal Transport Barrier (A. Fukuyama et al.)
5. Physics of Collapses - Probabilistic Occurrence of ELMs and Crashes - (S.-I. Itoh et al.)

Keywords: H-mode, improved confinement, transport barrier, radial electric field, transport suppression, collapses, ELMs, probabilistic excitation

Role of Nonuniform Superthermal Ions for Internal Transport Barriers

K. Itoh[1], T. Ohkawa [1,2], S.-I. Itoh[3], M. Yagi[3], A. Fukuyama[4]

[1] *National Institute for Fusion Science, Nagoya 464-01 Japan*
[2] *Department of Physics, UCSD, La Jolla CA, U. S. A.*
[3] *RIAM, Kyushu University, Kasuga 816 Japan*
[4] *Faculty of Engineering, Okayama Univ. Okayama 700, Japan*

Received 21 September 1997

Abstract
Influence of inhomogeneity of plasma flow on the magnetic surface, which is driven by the anisotropic hot ions, on the micro turbulence of the low/negative magnetic shear tokamak is investigated. It is found that the poloidal inhomogeneity is effective in suppressing the current-diffusive ballooning mode turbulence which has large nonlinear growth rate. This new mechanism of turbulence suppression provides the model of improved confinement associated with the reversed magnetic shear.

1. Introduction

After the theory of the electric field bifurcation for the H-mode [1] has been presented [2], the radial electric field structure are investigated widely [3-5]. (See the recent review [6].) In addition, the influence of the current profile on the confinement improvement has been studied experimental [7,8] and theoretical [9]. New type of the improved confinement in tokamaks with the reduced/negative magnetic shear, has been confirmed experimentally [10]. There are varieties in improved modes: the steep electron temperature gradient in JT-60U [11] suggests a new mechanism that drives the prominent transport barrier for electrons.

In this article we present a new mechanism of the suppression of the turbulence in the tokamaks with low/negative magnetic shear. We investigate the role of the toroidal plasma flow which is *inhomogeneous on the magnetic surface.* Such an inhomogeneity is sustained by the energetic ions which are inhomogeneous in the poloidal direction [12]. The nonlinear current-diffusive ballooning mode turbulence, which has been known to give understandings of the L-mode and high-β_p-mode [9] as well as the H-mode [13], is investigated. It is shown that the thermal conductivity of electrons and ions is substantially reduced. The necessary level of the poloidal-asymmetry of hot ions is derived.

2. Model Equation

A high aspect-ratio and cylindrical tokamak is employed and the quasi toroidal coordinates (r, θ, ζ) are used. The reduced set of equations [14] with electrostatic approximation is employed. When the hot ions are anisotropic, the perpendicular ion pressure, $p_{hot,\perp}$, could be dependent on the poloidal angle. We take into account of the poloidally-asymmetric hot ions, the pressure gradient of which is characterized as

$$\frac{\partial}{\partial\psi}p_{hot}(\psi, \theta) = \Gamma\,(1 + \cos\theta)\frac{\partial}{\partial\psi}p_0(\psi) \qquad (1)$$

In Eq.(1), ψ is the label of the magnetic surface (the minor radius here) and Γ is the parameter that indicates the magnitude. Combining the force balance equation of the electron fluid (Ohm's law), $\vec{E} + \vec{v} \times \vec{B} = \frac{1}{en}(-\nabla p_e + \vec{j} \times \vec{B})$, with the force balance equation

$\vec{j} \times \vec{B} = \nabla p_0 + \nabla p_{hot}$, the rotation velocity is obtained. When the energy of hot ions is much higher than that of bulk plasma particles, the poloidal inhomogeneity of the density is small and is neglected here. It is also assumed that the plasma is rotating in the toroidal direction, because the central plasma is of interest and the neoclassical damping of poloidal rotation is considered to be strong. Under this circumstance, the toroidal rotation frequency, $\Omega = V_\zeta / R$, is obtained [12] as $\Omega = \Omega_0(r) + \hat{\Omega}(r, \theta)$ with

$$\hat{\Omega}(\theta) = \Gamma (1 - \cos\theta) \frac{1}{e\bar{n}} \frac{dp_0}{d\psi} \simeq \left(\frac{\Gamma}{2} \frac{1}{e\bar{n}} \frac{dp_0}{d\psi} \right) \theta^2 + \cdots \qquad (2)$$

where we defined Ω_0 as $\Omega_0 = \Omega(\theta = 0)$. The toroidal angular velocity is not constant on the magnetic surface but has the poloidal inhomogeneity.

In the presence of this low, the nonlinear stability and the associated transport of the current-diffusive ballooning mode are analyzed, by use of the method of the dressed test mode. The mode with the toroidal mode number n is subject to the Doppler shift of $n\Omega$. Contrary to previous theories, not the radial inhomogeneity of $n\Omega$, but the poloidal inhomogeneity is studied. In the frame which is rotating with the angular frequency at $\theta = 0$, the Doppler shift is given by $n\Omega_t(\theta)$. This is a kind of the effect of the diamagnetic flow, but we here only keep the effect that will deform the mode structure along the field line. Thorough discussion on the diamagnetic and finite gyroradius effects will be discussed in a separate article [15]. By replacing the form of Doppler shift in the ballooning equation for the dressed test mode, [13], we have

$$\frac{d}{d\eta} \frac{F}{\tilde{\gamma} + \Lambda F^2} \frac{d}{d\eta} [\tilde{\gamma} + i\Delta\Omega + XF] \tilde{p} + \alpha (1 + \Gamma \cos\eta)(\kappa + \cos\eta + G \sin\eta) \tilde{p}$$
$$- [\tilde{\gamma} + i\Delta\Omega + MF] F [\tilde{\gamma} + i\Delta\Omega + XF] \tilde{p} = 0 \qquad (3)$$

where $\alpha = -q^2 R\beta'$, $s = rq'/q$,, q is the safety factor, R is the major radius, $\Lambda = \tilde{\lambda} n^4 q^4$, $K = \tilde{\chi} n^2 q^2$ and $M = \tilde{\mu} n^2 q^2$ represent nonlinear interactions. (Note that the length and the time is normalized to the minor radius a and poloidal Alfven time τ_{Ap}, respectively, as was in [13].) The metric factors $F = 1 + G^2$ and $G = s\eta - \alpha \sin\eta - (\alpha\Gamma/8) \sin 2\eta$ are modified by the poloidal asymmetry of pressure gradient, and the pressure gradient term also includes the Γ-correction as [16]. Perpendicular mode number is given as $k_\perp^2 = Fn^2 q^2$, and the relation $\lambda/\chi \simeq (\delta/a)^2$ holds. The normalized Doppler shift terms is expressed as $\Delta\Omega = \bar{\Omega}\, \theta^2/2$ with $\bar{\Omega} = nq\, \Gamma \left(- p_0' / e\bar{n} B_p v_A \right)$.

3. Self-Sustained Turbulence and Its Suppression

As in [13], Eq.(3) is approximated by the Weber-type equation assuming that the mode is localized near $\eta < 1$. In order to obtain the analytic insight, the limit of small α and s are analyzed, and Eq.(3) is expressed as

$$\left[\frac{d^2}{d\eta^2} + \frac{\Lambda}{X}\alpha \left(1 - \frac{MX}{\alpha} + \Gamma + \left(\frac{\alpha + X^2}{\alpha X} \right) i\omega \right) - \frac{\Lambda}{X}\alpha \left(1 + 2\Gamma + \left(\frac{\alpha + X^2}{\alpha X} \right) i\bar{\Omega} \right) \frac{\eta^2}{2} \right] \tilde{p}(\eta) = 0 \qquad (5)$$

$(\gamma \to -i\omega)$. This eigenmode equation is solved, and the nonlinear eigenvalue equation is given as

$$\frac{\Lambda}{X}\alpha - M\Lambda + \frac{\Lambda}{X}\alpha \left(\Gamma + \left(\frac{\alpha + X^2}{\alpha X} \right) i\omega \right) = \sqrt{\frac{1}{2} \frac{\Lambda}{X}\alpha \left(1 + 2\Gamma + \left(\frac{\alpha + X^2}{\alpha X} \right) i\bar{\Omega} \right)} \qquad (5)$$

Equation (5) is expanded with respect to Γ and $\tilde{\omega}$. In the limit of $\Gamma, \alpha \to 0$, solutions have been given as

$$\chi = \chi_L(s, \alpha \to 0) \simeq \frac{1}{\sqrt{2}} \frac{\lambda}{\chi} \sqrt{\frac{\chi}{\mu}}\, \alpha^{3/2} \qquad (6)$$

with $n^2q^2 = k_\theta^2 = (\chi/\lambda)\,\alpha^{-1}$ and $\alpha\Lambda/X \simeq 1$. Coefficients of the higher order are evaluated by use of the unperturbed solution, Eq.(6). Imaginary part of Eq.(5) gives

$$\omega = \frac{1}{2\sqrt{2}}\,\tilde{\Omega}\,. \tag{7}$$

Real part of Eq.(5) yields the transport coefficient. For a convenience, we introduce a coefficient C_1, which is of the order of unity, and write the coefficient of the $\tilde{\Omega}^2$ term as $(8\sqrt{2})^{-1}\sqrt{\Lambda\alpha/X}(\alpha/X + X/\alpha)^2 \equiv C_1 M\Lambda\,\alpha^{-1}$. With this simplification, Eq.(5) is simplified as

$$\frac{\Lambda}{X}\alpha - \sqrt{\frac{1}{2}\frac{\Lambda}{X}\alpha} - M\Lambda = M\Lambda\left(-\Gamma + \frac{C_1}{\alpha}\,\tilde{\Omega}^2\right) \tag{8}$$

If we compare this eigenvalue equation with the unperturbed one, the perturbed equation is obtained by the replacement as $\mu \rightarrow \mu\left(1 - \Gamma + C_1\alpha^{-1}\,\tilde{\Omega}^2\right)$. With this transformation, the transport coefficient, in the presence of asymmetric hot ions, is given as $\chi \simeq \left(1 - \Gamma/2 + C_1\,\tilde{\Omega}^2/2\alpha\right)^{-1}\chi_L$. The inhomogeneous rotation frequency and the asymmetric pressure gradient are related, and we have the relation $\tilde{\Omega} = (2q)^{-1}\sqrt{m_i/m_e}\;\Gamma$. By use of this relation, the suppression factor of the turbulent transport coefficient is finally given as

$$\frac{\chi}{\chi_L} = \frac{1}{\left(1 - \Gamma/2 + C_1\,\Gamma^2\Gamma_c^{-2}\right)} \tag{10}$$

with $\Gamma_c = 2\sqrt{2}\,q\sqrt{m_e/m_i}$. In the range of $\Gamma \sim \Gamma_c$, substantial reduction of the turbulent transport is expected. For the standard parameters, $q \simeq 1$ and $m_i/m_e \simeq 3600$ (i.e., Deuterium plasma), the critical asymmetry parameter Γ_c is approximately given as $\Gamma_c \simeq 0.05$. It is also noted that the critical value Γ_c is smaller for the DT-plasma compared to the D-plasmas.

The real frequency is given by Eq.(7). Noting the profile of the plasma rotation frequency, $\Delta\Omega = \tilde{\Omega}\,\theta^2/2$, Eq.(10) indicates that the phase velocity of the mode is close to the plasma velocity at $\theta \simeq 2^{-1/4}$(*radian*). The eigenmode is shown in Fig.1. Owing to the inhomogeneous toroidal rotation, the mode becomes weakly propagating, and the parallel mode number is increased.

This mechanism to reduce the turbulent transport is related with the "enhanced reduced shear mode". First, the nonlinear link between the transport coefficient and electron temperature works. If the electron temperature is increased and the hot ion

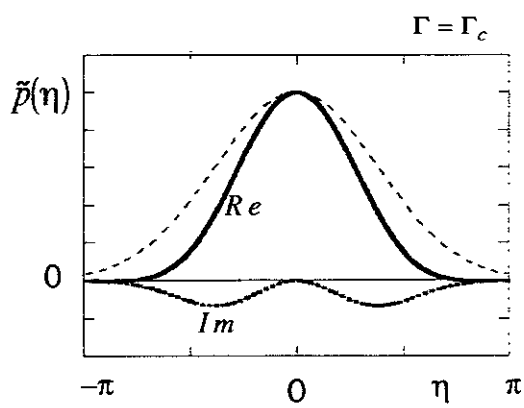

Fig.1 Eigenmode structure for the case of $\Gamma = \Gamma_c$. Solid line and dashed line show the real and imaginary parts, respectively. Thin and dotted line indicates the reference case with $\Gamma = 0$.

pressure builds up so as to exceeds the criterion Eq.(14), then the electron thermal conductivity as well as the ion's are reduced. By this reduced transport, the electron temperature further increases. The perpendicular injection of the beam ions is effective. Other key is the central localization of the heating profile. If the energetic ions are peaked, then the pressure gradient of hot ions is increased, giving larger Γ-parameters as is seen from Eq.(1). The peaked heating more easily causes the transport reduction of this article. Such a situation is realized in the JT-60U experiment, where the strong central heating is made by use of the perpendicular injection from the top and bottom. The absolute value of the toroidal rotation, Ω_0, is unimportant for this mechanism. It is noted that the cooperative phenomena appears with the reduced/negative magnetic shear. The weak-negative magnetic shear, combined with the Shafranov shift, causes the reduced transport [9]. The reduced transport by this new mechanism elevates the pressure gradient, and could enhance the Bootstrap current. The stronger the Bootstrap current, the larger the reduction of the magnetic shear so as to build up hot ions further. The reduced/negative magnetic shear is also effective from the view point of MHD stability. When the central q-value is lower than unity, the large amount of ions with large perpendicular energy could lead to the $m/n = 1/1$ mode instability such as the fish-bone mode [18]. If q is greater than unity, Γ could be high without causing such a deteriorating phenomena. These relations would explain the phenomena that the internal transport barrier of electrons was unambiguously observed in the reduced-negative magnetic shear operation of the JT-60U tokamak experiments.

4. Summary

In summary, we here theoretically analyzed the new mechanism of the reduction of turbulent transport in high temperature tokamaks. The new pattern of the plasma flow, i.e., the poloidal asymmetry of the toroidal flow, is investigated. The critical level of the asymmetric pressure gradient is obtained, and this mechanism is found to be very effective in reducing the turbulent transport of the electrons.

This work is partly supported by the Grant-in-Aid for Scientific Research of Ministry of Education, Science Sports and Culture of Japan, by the collaboration program of NIFS and by the collaboration program of Advanced Fusion Center of Kyushu University.

References

[1] Wagner F *et al* 1982: *Phys. Rev. Lett.* **49** 1408.
[2] Itoh S-I and Itoh K 1988 *Phys. Rev. Lett.* **60** 2276.
[3] Itoh S-I *et al.* 1989 in *Plasma Physics and Controlled Nuclear Fusion Research 1988* (IAEA, 1989, Vienna) Vol.2, p23.
[4] Shaing K C *et al* 1989 n *Plasma Physics and Controlled Nuclear Fusion Research 1988* (IAEA, 1989, Vienna) Vol.2, p13.
[5] Biglari H et al. 1990 *Phys. Fluids B* **2** 1.
[6] Itoh K and Itoh S-I 1996 Plasma Phys. Contr. Fusion **38** 1.
[7] Hugon M et al. 1992 *Nucl. Fusion* **32** 33.
[8] Koide Y et al. 1994 *Phys. Rev. Lett.* **72** 366.
[9] Fukuyama A et al 1994 *Plasma Phys. Contr. Fusion* **36** 1385
Fukuyama A et al. 1995 *Plasma Phys. Contr. Fusion* **37** 611.
[10] Levinton F M et al. 1995 *Phys. Rev. Let.* **75**, 4412.
Strait E J et al. 1995 *Phys. Rev. Let.* **75**, 4421
[11] Koide Y, et al. 1997 *Phys. Plasmas* **4** in press.
[12] Ohkawa T 1997 *Research Report* NIFS-484.
[13] Itoh S-I et al 1994 Phys. Rev. Lett. **72** 1200.
[14] Strauss H 1977 *Phys. Fluids* **20** 1354
[15] Itoh K, et al. 1997, paper in preparation.
[16] Sykes A et al. 1980 in *Plasma Physics and Controlled Nuclear Fusion Research* (IAEA, 1979, Vienna) Vol.1, p.625.
[17] Liu Chen, et al. 1984 *Phys. Rev. Lett.* **52** 1122.

Electric Field Bifurcation and Transition in the Core Plasma of CHS

A. Fujisawa, H. Iguchi, H. Sanuki, K. Itoh, S.-I. Itoh*, S. Okamura, K. Matsuoka, Y. Hamada

National Institute for Fusion Science, Oroshi-cho, Toki-shi, 509-52 Japan
*RIAM, Kyushu University , Kasuga 816 Japan

Abstract. In the CHS heliotron/torsatron, dynamic phenomena associated with transitions in radial electric field were observed during combined ECH+NBI heated plasmas. The observations with high temporal resolution confirmed a nonlinear relation between radial electric field and radial current to cause these phenomena associated with electric field bifurcation.

1. Introduction

The discovery of H-mode in ASDEX tokamak(Wagner *et al* 1982) has stimulated a research of better confinement regimes in toroidal helical plasmas(Erckmann *et al* 1993, Toi *et al* 1992). Bifurcation of radial electric field has been intensively discussed as a main working hypothesis to understand the H-mode physics is(Itoh *et al* 1988, Shaing *et al* 1989), and many experimental works have been extensively performed to investigate relation between the L-H transition and the electric field (Taylor *et al* 1989, Groebner *et al* 1990, Ida *et al* 1990, Weynants *et al* 1992, Burrel 1997). Experimental study of possible bifurcation of the radial electric field, which could happen spontaneously, has vital importance for understanding of confinement and structural formation in toroidal plasmas(Itoh and Itoh 1996).

In toroidal helical plasmas, transport can be enhanced by helically trapped particles, and the transport induced by helical ripple is intrinsically affected by the radial electric field(Kovrizhnykh 1984, Hastings 1985). Nonlinear dependence of the radial electric field allows the multiple equilibrium states in the toroidal helical plasmas, and can give birth to dynamic phenomena related to the radial electric field.

In the Compact Helical System (CHS) heliotron/torsatron, a heavy ion beam probe (HIBP) was installed to investigate the statics and dynamics of potential. The excellent temporal resolution allowed to observe a spontaneous transition in the radial electric field during a combined ECH+NBI heating phase(Fujisawa *et al* 1997). Here, we will describe these observations of dynamic phenomena associated with electric field bifurcation, and present obtained nonlinear relationship between radial electric field and current to induce the transition.

2. Experimental Set-up

The CHS is a medium size heliotron/torsatron device(Matsuoka et al. 1988). The present experiments were performed in the magnetic field configuration whose axis

is located on $R_{ax} = 92.1$cm, with its strength of 0.9T. The necessary beam is 71keV for this magnetic configuration in case that we use cesium. The HIBP adopts a unique method, which we call 'active trajectory control', to manage the beam trajectory(Fujisawa *et al* 1996). The method extends the accessible region of plasmas with different configurations. The observation location of HIBP is continuously altered by the sweep voltages to control the beam trajectory. The time evolution of potential profile can be observed by repeating a process of sweeping the voltages (radial scan mode), while fine temporal change in the potential at a spatial point can be detected by fixing the sweep voltage (fixed sweep mode).

3. Transition in Radial Electric Field

The first transition phenomenon was observed in a combined ECH+NBI heating phase of the CHS plasma. The target plasma is produced with 300kW ECH with its resonance on the magnetic axis. Then the neutral beam is injected into this plasma with port-through power of 800kW. The electron temperature is 800±200eV from a Thomson scattering system. The ion temperature is expected to increase from 100eV to 300eV. The electron density gradually changes from $n_e = 3 \times 10^{12}\text{cm}^{-3}$ to $n_e = 6 \times 10^{12}\text{cm}^{-3}$ during the combined heating phase.

Figure 1 shows the potential evolution at several spatial points in the combined ECH+NBI heating phase of the discharges. The data is taken in the fixed sweep mode for the sequential shots with an identical operational condition. A drastic change in potential occurs around $t = 55$ms. The potential at the plasma center exhibits abrupt drop by ~200V. It is followed by an abrupt rise by ~400V after a steady state in a short period of ~ 1ms. The timescale of this change can be also analytically obtained by fitting a function of $\tanh((t - t_0)/\tau)$ to the slopes. The analysis shows that the timescale parameters are $\tau = 60\mu$s and $\tau = 220\mu$s for the drop and rise, respectively. The timescale is much faster than the confinement time, which is a few milliseconds. The transition nature of the potential change is manifested in the fast timescale. At the location of the normalized radius of $\rho \simeq 0.3$, another rise and drop, that should be coincident with those at the plasma center, is observed around $t = 55$ms in a similar interval after the NBI turns on. On the other hand, no significant change can be seen outside of the radius of $\rho > 0.4$.

The structural change during the transition is also demonstrated in Fig. 1b. The solid (circles) and dashed lines show the potential profiles which were taken in the radial scan mode with an identical operational condition. Note that negative ρ means vertically lower half of the plasma. The timing when the beam scans the lowest and highest points are $t = 51.8$ms and $t = 58.2$ms, respectively. The profile indicated by the dashed line exhibits a unique feature that the electric field (e.g., its derivative) changes drastically inside and outside of $\rho = 0.4$. This steep gradient change suggests a momentum transport barrier. Profiles with this feature have been observed in plasmas with only ECH heating of 200 ~ 300kW.

The potential profile indicated by the circles shows clear asymmetrical peak in the upper half of the profile. This asymmetrical peak should be seen due to that the HIBP accidentally catches the potential change on the way of the back transition from the lower potential state to the higher one. The transition could not be caught since the beam scanned a point outside of $\rho = 0.4$ at the moment when the transition occurred. On the other hand, no significant difference in potential profiles taken in the radial scan mode has been found on the outside of $\rho = 0.4$. The closed and open

squares in Fig. 1c represent potential values taken in the fixed sweep mode, just before (t = 54.5ms) and after (t = 55.0ms) the transition, respectively. Thus, these facts support the proposition that the structural change of the transition should be localized in the plasma core.

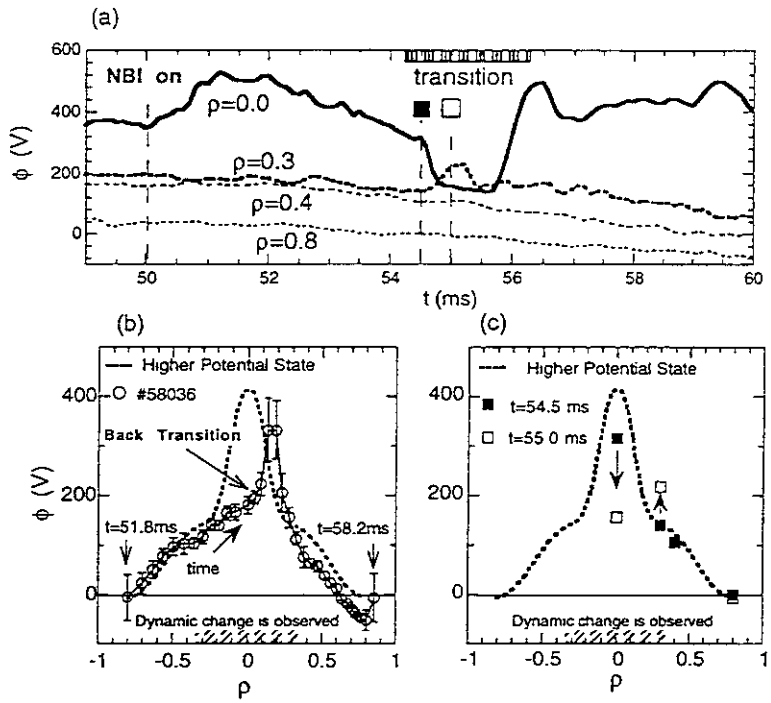

Figure 1. Transition observed in the combined ECH+NBI heating phase. (a) Time evolution of potentials at several spatial points. The transition occurs around t = 55ms. (b) Structural change in potential profile during the transition in a radial scan mode. The dashed and bold lines represents the potential profiles taken in the radial scan mode. (c) Structural change in potential profile during the transition. The losed an open squares indicate the potential changes observed in measurements with fixed points in Fig. 1a.

This transition is caused by nonlinear dependence of radial current on the radial electric field. The measured potential is transformed into the average radial electric field, which is defined as $\bar{E}_r = -(\phi(0.3a) - \phi(0))/0.3a$; here we make an assumption of $\phi(0.3a) = const.$ The radial current can be estimated in the following manner, $\epsilon_\perp \epsilon_0 \partial E_r/\partial t = -j_r$, where $\epsilon_\perp$ and ϵ_0 represent perpendicular and vacuum dielectric constants, respectively. In the present case, the perpendicular dielectric constant is $\epsilon_\perp \simeq 2.7 \times 10^4$. As a result, we can plot the radial current as a function of the electric field (E-J curve) in Fig. 2a. The arrows represent the direction of transition. The two curves for each transition are obtained in different methods to evaluate the electric field; wavelet analysis (solid line) and fitting method (dashed line). The error bars in the electric field and the radial current originate in uncertainty of potential change at $\rho = 0.3$. The above formula is a basic formula derived from a combination of the charge conservation law with the Poisson's equation.

A rough comparison with neoclassical theory should have some interests. Figure 2b shows neoclassical dependence of radial electric field on electron temperature. Plasma parameters used in the calculation are plausible for the experimental condition; T_i = 350eV $n_e = 5 \times 10^{12}\mathrm{cm}^{-3}$, $(\partial T/\partial\rho)/T = -0.6$ and $(\partial n/\partial\rho)/n = -0.3$. The other parameters, such as ε_h and ε_t, are selected for $\rho = 0.3$ in CHS. Multiple steady states are allowed when the electron temperature ranges from 630eV to 725eV. The transition

occurs from A to B, and from C to D. The radial current required for the transitions is plotted in Fig. 2c as a function of radial electric field. The maximum current to induce the transition is a few A/m^2, which is also within the experimental observations. Further investigations and accurate measurements of basic plasma parameters are essential for conclusive comparison.

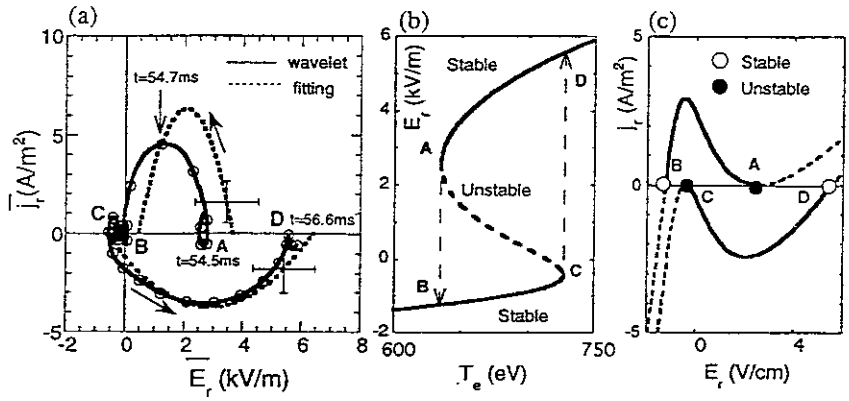

Figure 2. Nonlinear relationship between radial electric field and current. (a) Experimental nonlinear relationship between radial electric field and radial current. (b) Neoclassical dependence of radial electric field on electron temperature, and (c) nonlinear relation between radial electric field and radial current for the corresponding bifurcation conditions. The plasma parameter used in the calculation are $T_i = 350\text{eV}$ $n_e = 5 \times 10^{18}\text{m}^{-3}$, $(\partial T/\partial\rho)/T = -0.6$ and $(\partial n/\partial\rho)/n = -0.3$.

4. Summary

Dynamic phenomena related with transition are observed in the CHS heliotron/torsatron. The nonlinear relation to induce these phenomena is experimentally confirmed using a high temporal resolution of the HIBP.

References

Burrel K.H., Phys. Plasma 4, 1499(1997).
Erckmann V. *et al* Phys. Rev. Lett. **70** 2086(1993).
Fujisawa A. *et al* , *Rev. Sci. Instrum.* **67** 3099(1996).
Fujisawa A.*et al* , *Phys. Rev. Lett.* **79** 1054(1997).
Groebner J. ,Burrel K. H. and Seraydarian R. P., Phys. Rev. Lett. **64** 3015(1990).
Hastings D. E., Houlberg W. A., Shaing K. C., Nucl. Fusion **25**, 445(1985).
Ida K., Hidekuma S., Miura Y. *et al* , Phys. Rev. Lett. **65** 1364(1990).
Itoh S. -I., Itoh K., *Phys. Rev. Lett.* **63** 2276(1988).
Itoh K., Itoh S.-I., Plasma Phys. Cont. Fusion **36**, 1(1996).
Kovrizhnykh L. M., Nucl. Fusion **24**, 435(1984).
Matsuoka K. *et al* , 1989, *in Plasma Physics and Controlled Nuclear Fusion Research 1988*, (IAEA, Vienna), Vol.2, p411.
Shaing K. C., Crume Jr. E., *Phys. Rev. Lett.* **63** 2369(1989).
Taylor R. J., Brown M. L.,Fried B. D., Grote H., *et al* , *Phys.Rev. Lett.* **63** 2365(1989).
Toi K. *et al* , 1993. *in Plasma Physics and Controlled Nuclear Fusion Research 1992*(IAEA, Vienna) Vol.2, p461.
Wagner F. *et al* , Phys. Rev. Lett. **49** 1408(1982).
Weynants R. R. , Van Oost G. ,Bertschinger G. , *et al* , *Nucl. Fusion* **32** 837(1992).

Formation and termination of High ion temperature mode in Heliotron/torsatron plasmas

K.Ida[a)], K.Kondo[b)], K.Nagasaki[c)], H.Zushi[b)], Y.Kurimoto[d)], T.Hamada[d)], F.Sano[c)], T.Mizuuchi[c)], H.Okada[c)], S.Besshou[b)], H.Funaba[d)], S.Hidekuma[a)], K.Watanabe[a)], T.Obiki[c)]

(a)National Institute for Fusion Science Oroshi-cho, Toki-shi, Gifu, 509-52, Japan
(b)Graduate School of Energy Science, Kyoto University, Uji, 611, Japan
(c)Institute of Advanced Energy, Kyoto University, Uji, 611, Japan
(d)Faculty of Engineering, Kyoto University, Kyoto, 606-01, Japan

Physics of the formation and termination of High ion temperature mode (high T_i mode) are studied by controlling density profiles and radial electric field. High ion temperature mode is observed for neutral beam heated plasmas in Heliotron/torsatron plasmas (Heliotron-E). This high T_i mode plasma is characterized by a peaked ion temperature profile and is associated with a peaked electron density profile produced by neutral beam fueling with low wall recycling. This high T_i mode is terminated by flattening the electron density caused by either gas puffing or second harmonic ECH (core density "pump-out").

1. Introduction

Improved confinement modes, H-mode, high T_i mode, and reheat mode have been observed in Heliotron/torsatrons and in stellarators as well as in tokamaks[1]. There are similarities between the high T_i mode in Heliotron/torsatron and super shots in TFTR [2], hot ion modes in JET and in JT-60 [3,4]. These improved confinement modes are characterized as high ion temperature (low ion thermal diffusivity) and peaked density profiles, although the electron transport has no significant improvement. The causality between density peaking and improvement of ion transport (ion thermal barrier) is studied in Heliotron-E high T_i mode discharges.

Heliotron-E is an axially asymmetric heliotron/torsatron with l=2 , m=19, major radius R=2.2m, minor radius a = 0.2m, magnetic field B=1.9T, NBI power < 3MW [5]. The time evolution of ion temperature profiles are measured with multi-chord charge exchange spectroscopy (TVCXS) with 40 spatial channels and with a 16.7ms time resolution using a charge exchange recombination line of fully stripped carbon [6]. Fast changes in the central ion temperature are measured with a center chord neutral particle analyzer (NPA) with a time resolution of 2 ms. The density peakedness is estimated with 7-chord FIR interferometer [7]. Time evolution of the central electron temperature is measured with electron cyclotron emission(ECE), while the radial profile of electron temperature is measured with Thomson scattering.

2. High T_i mode discharge

As expected from a density dependence of energy confinement time of $\tau_E \propto n_e^{0.7 - 1.0}$ in heliotron/torsatron devices, temperature has a weak dependence on plasma density in L-mode. No dependence of ion temperature on electron density in the plateau regime has been reported[8]. Therefore when the electron density increases in time with gas puffing, the ion temperature stays almost constant or decreases gradually in the L-mode discharges. However, when the gas puff is turned off after the neutral beam injection with low wall recycling due to boron coating, both central electron density, $n_e(0)$, and central ion temperature, $T_i(0)$, increase in time and the central ion temperature reaches almost two times higher than that in the L mode discharges with similar central electron density as seen in Fig. 1(a). These discharges are characterized by a peaked ion temperature

profile and are associated with a peaked electron density profile produced by neutral beam fueling with low wall recycling, which is called the high T_i mode[9]. As seen in the ion temperature profile in Fig.1(b), there is no localized thermal barrier observed in the high T_i mode. The formation of the thermal barrier in high T_i mode is considered to be gradual in time and broad in space, since the increase of central ion temperature is 30 - 40 ms and much longer than the global energy confinement time (6ms in L mode and 9ms in the high T_i mode plasma).

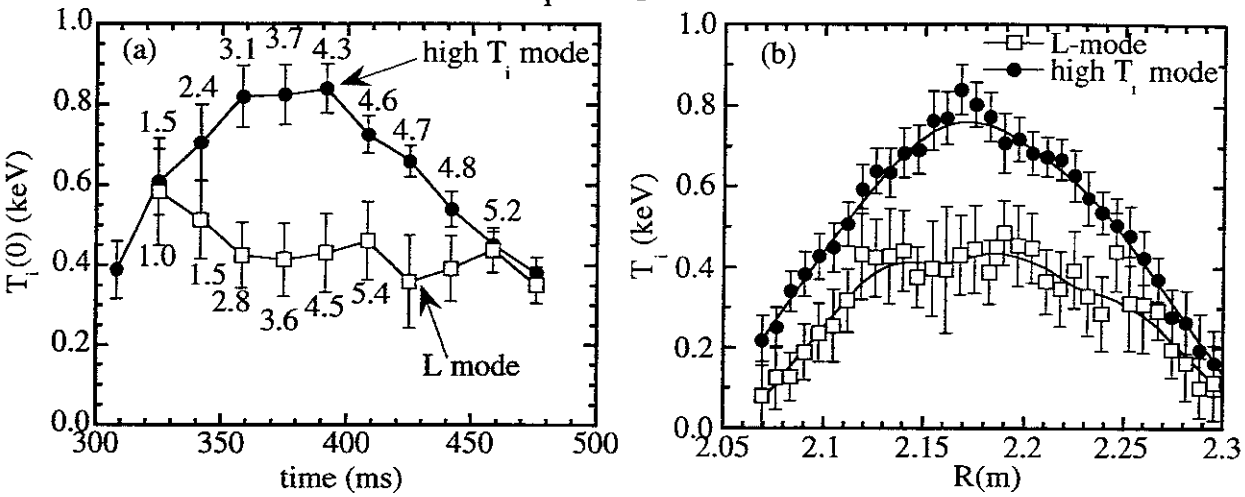

Fig.1 (a) Time evolution of central ion temperature and (b) radial profile of ion temperature at t = 390 ms for the high T_i mode and L mode discharge in the Heliotron-E. The values of central electron density are illustrated in Fig.(a) in the unit of 10^{19} m^{-3}.

3. Termination of high T_i mode by adding the second harmonic ECH pulse

Second harmonic ECH has particle "pump-out" in the core region and makes the density profiles flat [10]. When the 2nd-ECH is applied to a plasma with peaked density profile, both the density peakedness and central ion temperature decrease, although the total heating power by NBI plus ECH is increased. As seen in Fig. 2(a), the central electron temperature increases in a time scale on the order of energy confinement time (~ 6 - 9 ms) while the central ion temperature starts to decrease slowly in the time scale of more than 40ms, when the 2nd-ECH pulse is turned on in the high T_i mode discharge. The time scale for the recovery of central ion temperature after the ECH pulse is turned off has a similar value.

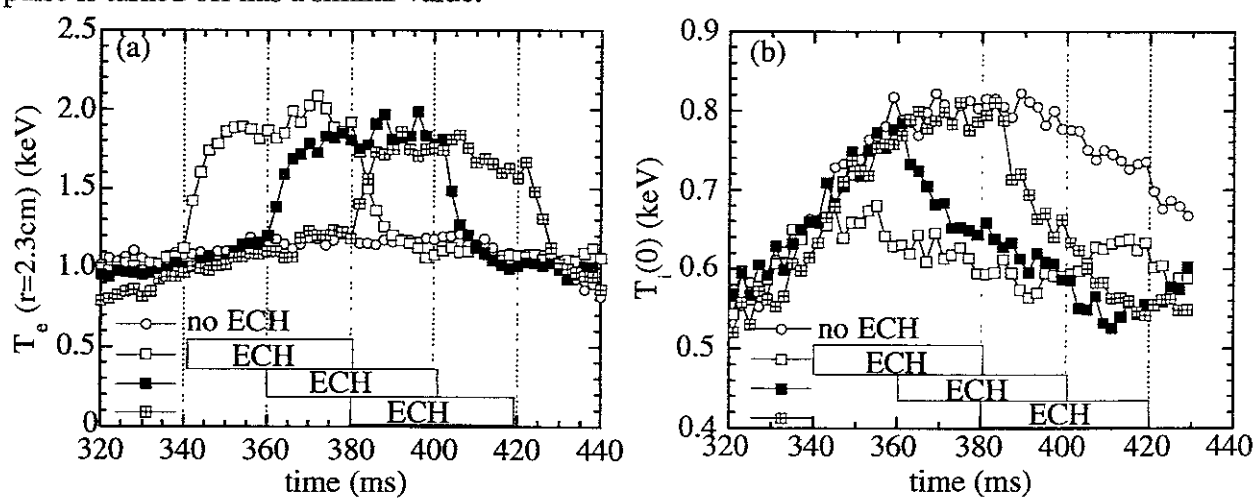

Fig.2 Time evolution of (a) electron temperature near plasma center (r=2.3cm) measured with ECE and (b) the ion temperature measured with neutral particle analyzer (NPA) for the high T_i mode discharge (no ECH pulse) and the discharges with 2nd harmonic ECH pulse for t = 340-360ms, 360-400ms, and 380-420ms in the Heliotron-E.

As shown in Fig. 3, the drop of ion temperature due to the 2nd harmonic ECH is observed in the plasma core ($\rho < 0.6$) , where significant increase of the electron temperature is observed. Since both the NB heating power to ions and energy flow from electrons to ions increase by adding 2nd harmonic ECH, the drop of ion temperature should be due to the enhancement of ion thermal diffusivity, χ_i. As seen in Fig.3(c), the change in the ion thermal diffusivity, χ_i at the formation of high T_i mode and termination of high T_i mode (high T_i + 2nd ECH) is mainly at the plasma core of $\rho < 0.6$. When the 2nd harmonic ECH terminates the thermal barrier by degrading the density peaking, the central ion thermal diffusivity at $\rho = 0.1$ is enhanced from ~ 0.5 m^2/s to ~ 10 m^2/s, which value is even higher than that in L- mode discharges (~ 2 m^2/s).

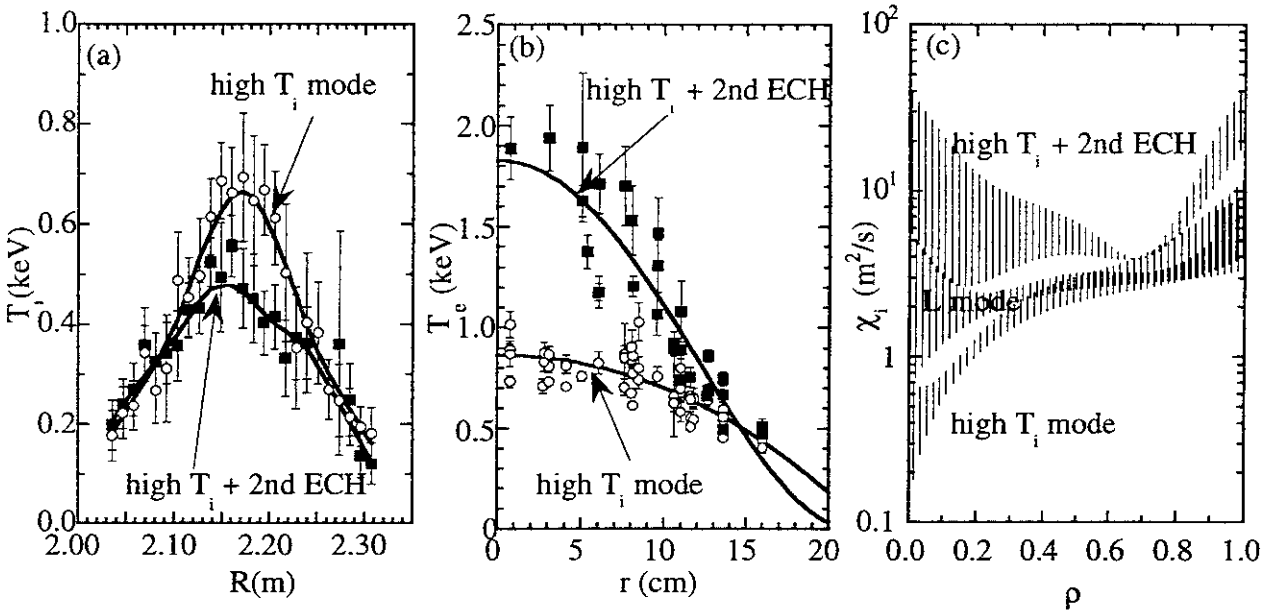

Fig.3 Radial profiles of (a) ion temperature, (b) electron temperature, and (c) ion thermal diffusivity for high T_i mode discharge (t = 375ms) and the high T_i + 2nd ECH discharge (t = 390ms) where the 2nd harmonic ECH is added to the high T_i mode discharge for t = 360 - 400ms. The radial profile of thermal diffusivity for low density L-mode is also plotted in Fig(c) as a reference.

4. Causality between electron temperature rise, density peaking and ion temperature drop

The formation and termination of the high T_i mode described above are associated with the flattening of the density profile. To study a causal link between the electron temperature rise due to ECH, increase of density gradient and improvement of ion transport, we measured the time evolution of the central electron temperature, the density peakedness and the central ion temperature at the onset of the 2nd-ECH pulse for the high T_i mode discharges, where both the electron density and ion temperature are peaked.

Figure 4 shows the density peaking factor as a function of the central electron temperature and the central ion temperature as a function of the density peaking factor. If both the electron temperature rise and density flattening and the density flattening and drop of central ion temperature take place simultaneously, this is the case that the 2nd harmonic ECH directly degrades both particle and heat transport (and particle and heat transport have similar magnitudes), and therefore each time trace should be on one line. When there is causality between these two parameters, the time trace deforms to be elongated circularly and the direction of rotation (clockwise or counter clockwise) shows which is first. Fig.4(a) shows that the increase of electron temperature is first followed by density peaking and then finally by the drop in the ion temperature. The change of electron temperature is observed only just after the ECH pulse is turned on (t = 300 - 306 ms), the density peaking and ion temperature

drop take 18ms and 40ms (or more), respectively. Similar characteristics are observed more clearly after the 2nd ECH is turned off. At t = 410ms, the electron temperature already has gone back to the level before the ECH pulse, the density profile stays flat and ion temperature still keep decreasing. The recovery of the density peaking and ion temperature are observed with time delays of 10ms and 20 ms, respectively. These observations support the hypothesis that the increase of electron temperature causes the density flattening and the flattening of density profiles causes the drop in ion temperature and the enhancement of the ion thermal diffusivity. The large ion thermal diffusivity for the discharges with a 2nd ECH pulse [see Fig.3(c)] is also explained by this mechanism.

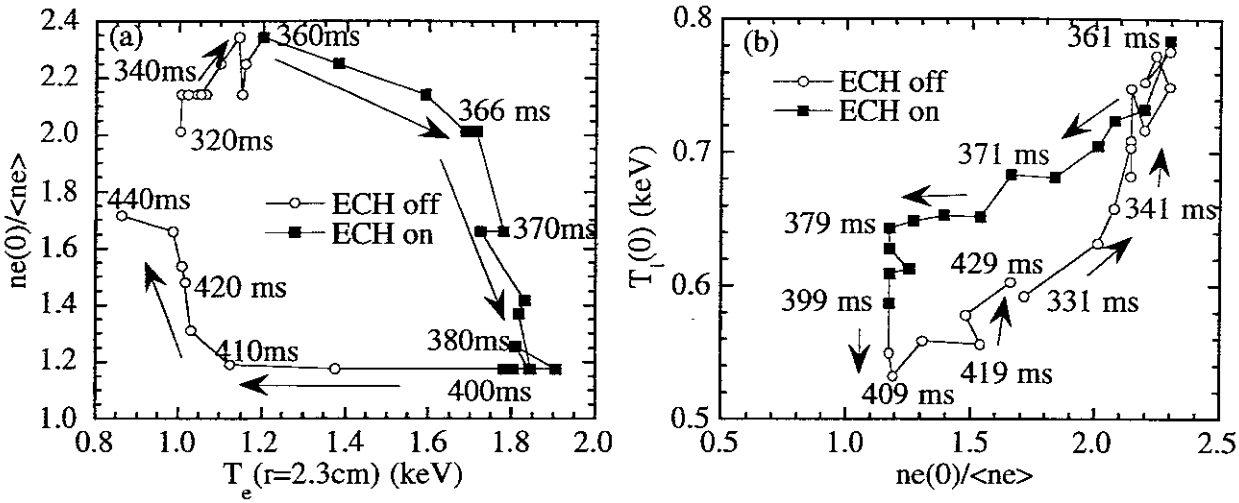

Fig.4 Time evolution of (a) peaking factor of electron density profiles as a function of central electron temperature and (b) central ion temperature as a function of peaking factor of electron density profiles for the discharge with 2nd harmonic ECH pulse for t = 360-400ms in the Heliotron-E.

The important effect of density peaking is its enhancement of the radial electric field shear, because the bulk rotation tends to remain constant [11]. Since radial electric field measurements with charge exchange spectroscopy have a relatively poor time resolution of 17ms, it is difficult to study the causality link between the formation of radial electric field shear and improvement of ion thermal transport. However, the radial electric field shear is observed in the steady state phase of high T_i mode, while there is no radial electric field shear observed in L mode[9]. Therefore the flattening of density profiles after 2nd ECH is turned on imply the disappearance of radial electric field which contributes to the ion transport improvement in the high T_i mode phase. The authors acknowledge technical support by the Heliotron-E, ECH, NBI, and machine operation groups. The authors acknowledge useful discussion with Dr.B.J.Peterson.

References

[1] A.Iiyoshi, et al., in Plasma Phys. and Control. Nucl. Fusion Research (Porc. 16th Int. Conf. on plasma phys. and Contl. Nucl. Fusion Research, Montreal, 1996) IAEA Vienna (1997).
[2] R.J.Fonck, et al., Phys. Rev. Lett. **63**, 520 (1989).
[3] H.Weisen et al., Nucl. Fusion **29**, 2187 (1989).
[4] Y.Koide, et al., Nucl. Fusion **33**, 251 (1993).
[5] F.Sano, et. al., Nucl. Fusion **30** (1990) 81.
[6] K.Ida, S.Hidekuma, Rev. Sci. Instrum. **60**, (1989) 867.
[7] H.Zushi, et. al., Nucl. Fusion **27** (1987) 286.
[8] K.Ida, et al., Phys Fluids B 4 (1992) 1360.
[9] K.Ida, et al., Phys. Rev. Lett. **76** (1996) 1268.
[10] T. Mizuuchi, et al., in Controlled Fusion and Plasma Physics (Proc. 23rd Eur. Conf. Kiev, 1996) European Physical Society.
[11] K.Ida, et al., Plasma Phys. 38 (1996) 1433.

Transition to an Enhanced Internal Transport Barrier

A Fukuyama†, S. Takatsuka†, S-I Itoh‡, M Yagi‡ and K Itoh§

† Faculty of Engineering, Okayama University, Okayama 700, Japan

‡ Research Institute for Applied Mechanics, Kyushu University, Kasuga, Fukuoka 816, Japan

§ National Institute for Fusion Science, Toki 509-52, Japan

Abstract. The role of $E \times B$ rotation shear in the internal transport barrier formation is examined by means of a one-dimensional transport simulation based on the current-diffusive ballooning mode turbulence model. Delayed transition to the enhanced improved transport was reproduced in the medium heating power range. The threshold power is strongly reduced by the effect of rotation shear. Simulation including particle transport was also applied to NBI-heated plasmas and the steepness of density and temperature gradients is discussed.

1. Introduction

Various operation modes of improved core confinement have been observed on tokamaks and comprehensive modelling of the internal transport barrier (ITB) is urgently required for. The transport model [1] based on the self-sustained turbulence of the current-diffusive ballooning mode (CDBM) has made a success in describing the L-mode scaling and improved confinement modes associated with ITB in a core plasma [2, 3]. The reduction of the thermal diffusivity χ_{CDBM} derived from the CDBM model explains the formation of ITB where the magnetic shear is weak or negative and/or the Shafranov shift due to pressure gradient is large. In the region of steep ion pressure gradient near the ITB, radial force balance leads to a large radial electric field. It has been shown [4] that the $E \times B$ rotation shear also reduces χ_{CDBM}. This additional mechanism introduces another time scale and may lead to transition to a state of enhanced confinement.

In this paper, we describe the transport model including the effect of $E \times B$ rotation shear and simulate the delayed transition to the core confinement and the density peaking which are usually observed in experiments.

2. Transport Model Including $E \times B$ Rotation Shear

In the self-sustained turbulence model of CDBM, turbulent-induced current diffusivity destabilizes the ballooning mode, while ion viscosity and thermal diffusivity which are

also induced by turbulence stabilize the mode. The thermal diffusivity derived from the marginal stability condition is expressed as [2, 4]

$$\chi_{\rm CDBM} = C\,\frac{F(s,\alpha,\kappa)}{1+G\omega_{E1}^2}\,\alpha^{3/2}\frac{c^2}{\omega_{\rm pe}^2}\,\frac{v_{\rm A}}{qR} \tag{1}$$

where the normalized pressure gradient, $\alpha \equiv -q^2R(\mathrm{d}\beta/\mathrm{d}r)$, magnetic curvature, $\kappa \equiv -(r/R)(1-1/q^2)$, magnetic shear, $s \equiv (r/q)\,(\mathrm{d}q/\mathrm{d}r)$ and rotation shear, $\omega_{E1} \equiv (\tau_{\rm Ap}/sB)\,(\mathrm{d}E_r\mathrm{d}r)$. The factor $F(s,\alpha,\kappa)$ represents the reduction due to weak or negative magnetic shear and large Shafranov shift. The reduction by $1/(1+G\omega_{E1}^2)$ is the effect of $E\times B$ rotation shear. Although the factor G is also a function of s and α, we approximate it by a constant parameter $G=10$ in the following calculation.

We solve the one-dimensional transport equations

$$\frac{\partial}{\partial t}n_s = -\frac{1}{r}\frac{\partial}{\partial r}r\Gamma_s + S_s, \qquad \frac{\partial}{\partial t}\frac{3}{2}n_sT_s = -\frac{1}{r}\frac{\partial}{\partial r}rq_s + P_s,$$

$$\frac{\partial}{\partial t}B_\theta = \frac{\partial}{\partial r}\eta_{\rm NC}\left[\frac{1}{\mu_0}\frac{1}{r}\frac{\partial}{\partial r}rB_\theta - J_{\rm BS}\right]$$

with the radial flux

$$\Gamma_s = n_sV_s - D\frac{\partial}{\partial r}n_s, \qquad q_s = \frac{5}{2}n_sT_sV_s - \frac{3}{2}n_s\chi_s\frac{\partial}{\partial r}T_s$$

The transport coefficients are expressed as a sum of neoclassical contribution and $\chi_{\rm CDBM}$;

$$V_s = n_s\left(v_{\rm Ware} - 0.05\,\chi_{\rm CDBM}\frac{r}{a^2}\right), \qquad D = D_{\rm NC} + 0.1\,\chi_{\rm CDBM}$$

$$\chi_{\rm e} = \chi_{\rm NC,e} + \chi_{\rm CDBM}, \qquad \chi_{\rm i} = \chi_{\rm NC,i} + \chi_{\rm CDBM}$$

and fitting parameter C in eq.(1) was chosen to be 8. The difference of C with [2] is due to the factor 3/2 in the right hand side of eq.(4).

3. Results of Transport Simulation

We have carried out heat transport simulation of the high-$\beta_{\rm p}$ mode with fixed density profiles. Figure 1 shows the comparison of temperature evolution without and with the effect of $E\times B$ rotation shear for $R=3\,\mathrm{m}$, $a=1\,\mathrm{m}$, $B=3\,\mathrm{T}$, $I_{\rm p}=1\,\mathrm{MA}$, $n_{e0}=0.5\times10^{20}\,\mathrm{m}^{-3}$. Without the effect of rotation shear, we need heating power of 10 MW for high $\beta_{\rm p}$ improved confinement [2]. We found strong reduction of the threshold power and increase of the confinement improvement factor with the effect of rotation shear. Delayed transition to an enhanced confinement state was observed for the heating power slightly above the threshold value. About one second after the onset of additional heating, internal transport barrier is formed and the stored energy of the plasma starts to grow again. The delay is caused by gradual increase of the pressure gradient and modification of the current profile. The transport barrier does not move inward as was observed in the high-$\beta_{\rm p}$ mode without the effect of rotation shear. In some cases, oscillation of the outward heat flux due to the change of the ITB strength was observed.

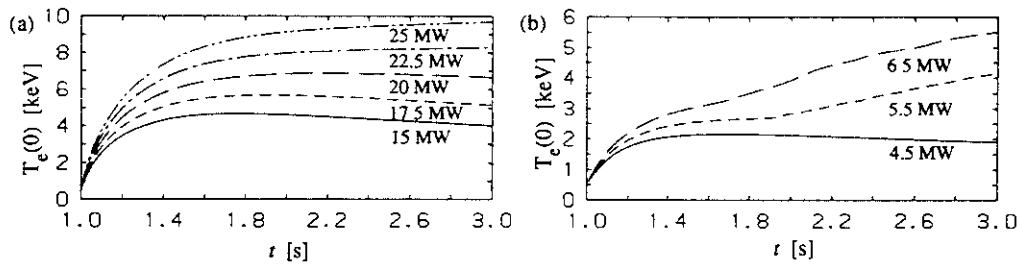

Figure 1. Time evolution of T_{e0} without (a) and with (b) the effect of rotation shear.

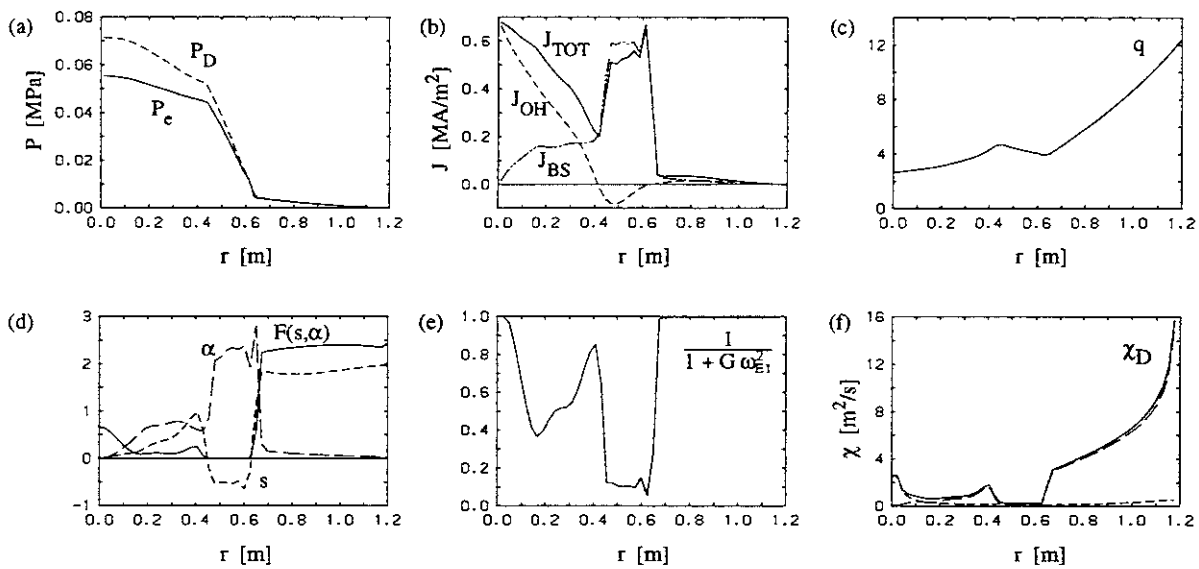

Figure 2. Radial profiles at $t = 3\,\mathrm{s}$ with the $E \times B$ rotation shear effect.

In the negative shear configuration, steep gradient of density profile as well as temperature profiles has been observed at ITB. In order to simulate the experiment on JT-60U [6], we have included particle transport which was not taken into account in our previous simulation [3]. Figure 3 shows time evolution for $R = 3.15\,\mathrm{m}$, $a = 0.74\,\mathrm{m}$ and $B = 4.28\,\mathrm{T}$. The plasma current was increased from 0.6 MA to 2 MA and NBI heating of 12 MW was switched on at $t = 1\,\mathrm{s}$. After the switch on, the central and volume-averaged densities start to grow. The temperatures as well as the bootstrap current I_{BS} also start to increase but decline for $t > 1.8\,\mathrm{s}$. Radial profiles at $t = 1.8\,\mathrm{s}$ are shown in Figure 4. The density and temperature profiles are very close to experimental observations [6]. Large bootstrap current is generated owing to the steep density gradient. Negative magnetic shear due to off-axis current, large Shafranov shift due to large total pressure gradient and $E \times B$ rotation shear due to large ion pressure gradient contribute to reduce the transport within the ITB. The main difference between the experiment and the simulation is the decline of temperature during the NBI heating. The stored energy and the density increase almost linearly with time in the experiment. The decrease of stored energy in simulation is attributed the shrink of ITB radius due to insufficient heating power.

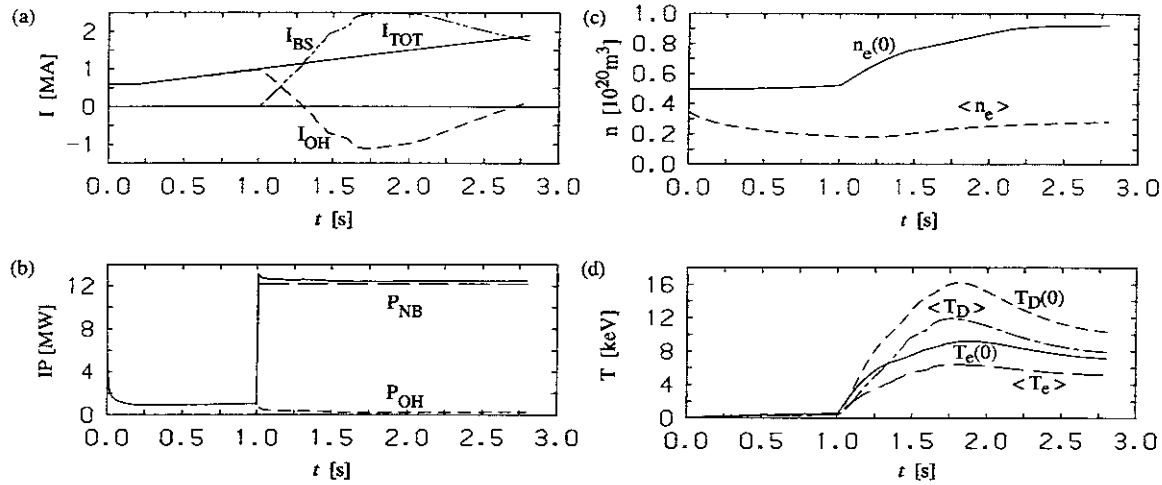

Figure 3. Time evolution in the negative shear configuration.

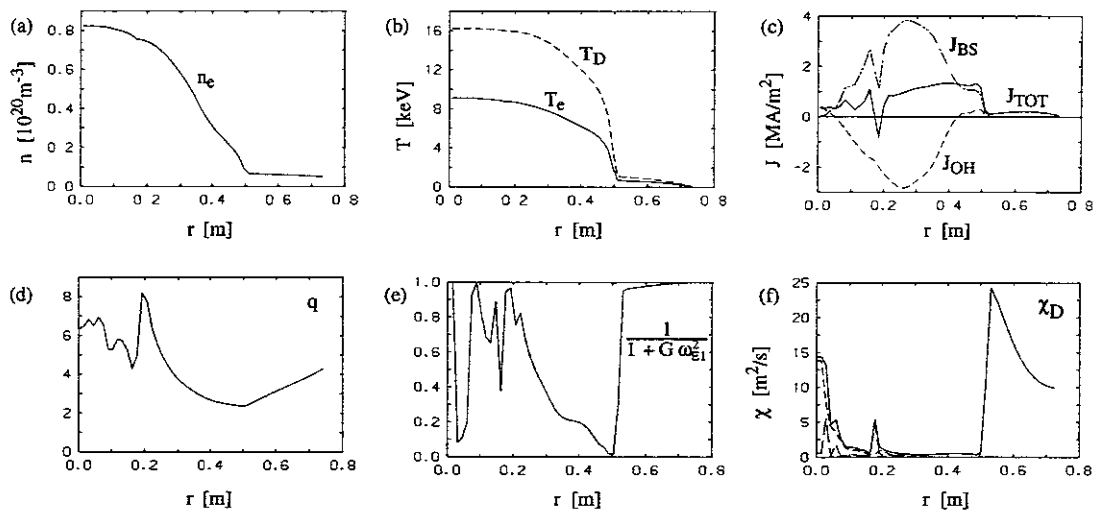

Figure 4. Radial profiles at $t = 1.8$ s in the negative shear configuration.

4. Summary

Reduction of transport due to $E \times B$ rotation shear is included in the transport simulation based on the CDBM turbulence transport model. The rotation shear effect strongly reduces the threshold power for ITB formation and explains delayed transition to the enhanced confinement state. Transport simulation including density evolution indicated density, temperature and safety factor profiles very close to experimental observations.

[1] Itoh K 1994 *Plasma Phys. Control. Fusion* **36** 279; *ibid.* 1501
[2] Fukuyama A, *et al.* 1995 *Plasma Phys. Control. Fusion* **37** 611-31
[3] Fukuyama A *et al.* 1995 *Nucl. Fusion* **35** 1669
[4] Itoh S-I *et al.* 1996 *Plasma Phys. Control. Fusion* **38** 1743
[5] Levinton F M *et al.* 1996 *Proc. of 6th IAEA Conf. on Fusion Energy* IAEA-CN-64/A1-3
[6] Fujita T *et al.* 1996 *Proc. of 6th IAEA Conf. on Fusion Energy* IAEA-CN-64/A1-4

Physics of Collapses
- Probabilistic Occurrence of ELMs and Crashes -

S.-I. Itoh, S. Toda*, M. Yagi, K. Itoh†, A. Fukuyama††

Research Institute for Applied Mechanics, Kyushu U. 87, Kasuga 816, Japan
** Interdisciplinary Graduate School of Engineering Sciences, Kyushu U., Kasuga 816 Japan*
† National Institute for Fusion Science, Nagoya 464-01, Japan
†† Faculty of Engineering, Okayama University, Okayama 700, Japan

Received 22 September 1997

Abstract

Statistical picture for the collapse is proposed. The physics picture of the crash phenomena, which is based on the turbulence-turbulence transition, is extended to include the statistical variance of observables. The dynamics of the plasma gradient and the turbulence level is studied, with the hysteresis nature in the flux-gradient relation. The probabilistic excitation is predicted. The critical condition is described by the statistical probability.

I. Introduction

Collapse phenomena are widely observed in various toroidal confinement devices. The collapses of transport barriers require understanding of the formation of the barrier as well as the physics mechanism to cause its decay. The MHD instabilities have been nominated as the main mechanism for the onset of the collapse. The key to understand the mechanism is the trigger, i.e., the abrupt and discontinuous change of the growth rate of fluctuations, which leads to the crash of global structure. This feature clearly shows that the collapse is a nonlinear phenomenon and cannot be explained by the linear stability analysis [1].

A model has been proposed that these collapse events are due to the turbulence-turbulence transition. The M-mode transition, i.e., that to the magnetic braiding mode, gives rise to the hysteresis characteristics in the gradient-flux relation. When the pressure gradient (α) exceeds the threshold, the M-mode transition sets in, and the bursting of energy appears owing to the faster anomalous transport than that in the L- and H-mode. We attribute the M-mode transition to the models of Giant ELMs [2], internal transport barrier collapse [3], sawtooth [4] and minor disruptions [5]. The picture of transition seems to explain the observed phenomena in experiments [1]. Generally, the transition (bifurcation) is modelled by the Ginzburg-Landau type equation which includes the nonlinear bifurcation. In the case of the L-H transition study, the model equation is tested to explain the experimentally-observed dithering ELMs [6]. The study clearly demonstrates that the high temperature plasma has a transition nature.

Based upon these knowledge we here explore a new aspect associated with the transition. The aspect is the probabilistic nature of its occurrence. Usually, the dynamics of transition in confined plasmas has been studied based on the deterministic view of the events. The critical condition of the onset has been discussed. However, similar to the transition characteristics in other area of physics, there exist statistical variances in the relevant variables. The statistical variance affects the transition nature and introduces a change from the deterministic phenomenon to the probabilistic one. In this paper, we shall show the probabilistic nature of the transition by using the zero-dimensional (0-D) dynamical model. Various origins of statistical variance are considered.

II. Zero-Dimensional (0-D) Dynamical Model of Transition

The dynamical model of transition has been studied in many literature [7]. We here adopt two basic equations: One is the evolution of global structures (say, gradient) and the other is the dynamics of the loss rate that produces the hysteresis of the flux-gradient relation. We take two representative variables, i.e., the pressure gradient α and the loss rate γ. The loss rate is directly related to the turbulence level.

The reduction to the 0-D model from the transport equation has been discussed [8]. A layer with a finite width is considered, and the averaged value within this layer is treated as a scalar quantity. The hysteresis property is modelled by the Ginzburg-Landau model, i.e., the cubic

formula. Though highly simplified, the GL model form of the hysteresis has successfully applied to the investigation of the dynamics of ELMs. The model equation takes the form

$$\frac{\partial}{\partial t}\alpha = S - \gamma\alpha \tag{1}$$

$$\zeta\frac{\partial}{\partial t}\gamma = \alpha - 1 + a(\gamma - 1) - b(\gamma - 1)^3 \tag{2}$$

The notation is as follows: S is the energy influx into the layer, ζ denotes the possible of dynamical time difference between α and γ; the cubic equation $a(\gamma-1)-b(\gamma-1)^3$ describes the shape of the hysteresis in the gradient-flux relation.

The dynamical nature of the set of equations has been studied. If all the coefficients (S, a, b, ζ) are constant in time, Eqs.(1) and (2) predict the converging stable stationary solutions or the dynamical solution of a limit cycle. Stationary solutions are obtained for (1) $S < S_1$ (lower flux branch), $S_2 < S$ (higher flux branch), and a limit cycle appears for $S_1 < S < S_2$, $(S_1 = \left(1 - \sqrt{a/3b}\right)\left\{1 + (2a/3)\sqrt{a/3b}\right\}$ and $S_2 = \left(1 + \sqrt{a/3b}\right)\left\{1 - (2a/3)\sqrt{a/3b}\right\})$.

As the physics origin of the transport, the turbulence level is often discussed in terms of the statistical averages. The relation between its averaged level and the gradient of the global plasma parameter has been a main subject of the plasma physics. The turbulence level is also associated with the statistical variance. This is true even in a thermal equilibrium, and the Gaussian statistics is used. For the confined plasmas, which is far from thermal equilibrium, the statistical variance is as important a quantity as the statistical average. The nonlinear simulation has shown a large temporal variation around the average [9]. The experimental observation has demonstrated that the statistical deviation from the mean value could be as large as the average itself [10]. Based on these considerations, we consider that parameters (S, a, b) are statistical variables and have fluctuation parts in time. For instance, the heat flux into the region of subject could fluctuate in time with some statistical distribution. The temporal variation of the relevant magnetic perturbation amplitude has a statistical nature. These processes give the statistical nature of (S, a, b). We put

$$S = S_0 + \varepsilon_f, \qquad a = a_0 + \varepsilon_a \tag{3}$$

and consider ε_f and ε_a as statistical variables, e.g., $\langle\varepsilon_a\rangle = 0$ and $\langle\varepsilon_a^2\rangle \neq 0$. The variance ε_f represents that of the fluctuations of the source from upstream. The variance ε_a comes from the deviation from the mean fluctuation level that is relevant for the onset of the magnetic braiding in the region of interests.

III. Probabilistic Transition

Temporal evolution is studied based on Eqs.(1) and (2). Figure 1 shows the periodic

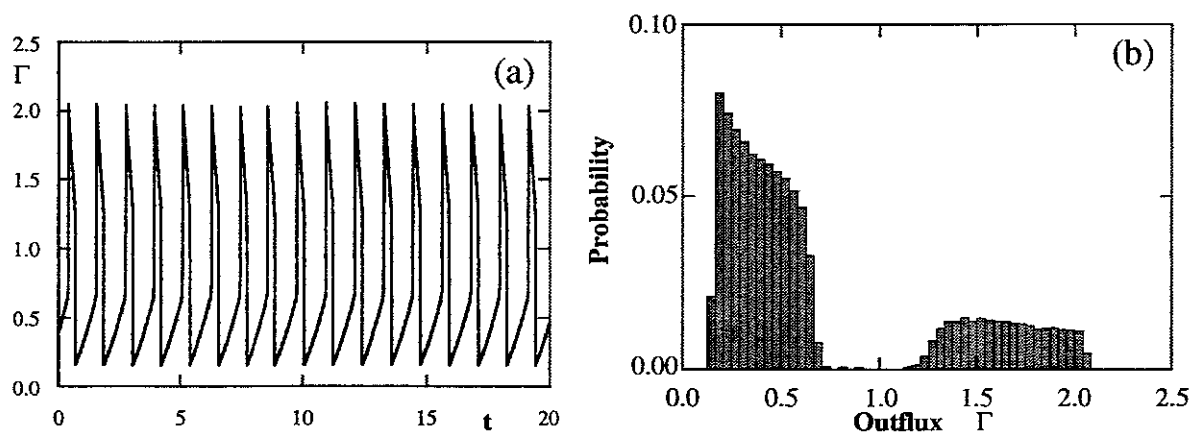

Fig.1 Time evolution of the periodic burst of the plasma loss (a) and the distribution function of the loss flux (b) in the absence of statistical deviations.

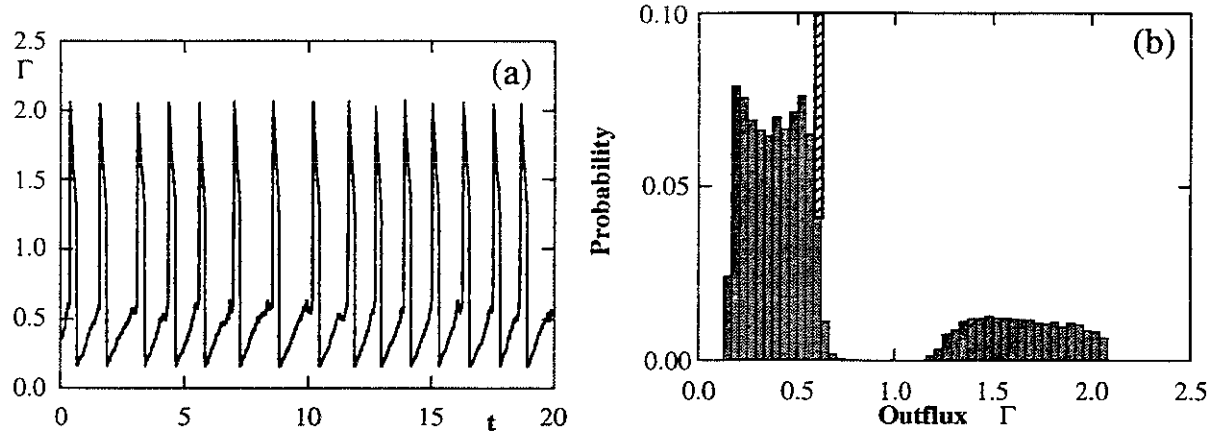

Fig.2 Irregular bursts are excited in the presence of the statistical deviations. Temporal evolution (a) and distribution function (b). In the absence of the random part of the source periodic bursts are not possible and distribution becomes like a delta-function (shaded bar in (b)).

solution of the out flux $\Gamma = \gamma\alpha$ for the case of constant coefficients (S, a, b). The distribution function of the observed value of Γ is also plotted. The parameters are chosen as $a = 0.5$, $b = 1$, and $\zeta = 0.01$, so that the critical fluxes are given as $S_1 \simeq 0.67$ and $S_2 \simeq 1.21$. In the case of Fig.1, S_0 is chosen as $S_0 = 0.7$, and the time trace of the limit cycle exhibits the existence of the higher flux range. If we choose $S_0 = 0.6$, for the other fixed parameters, no oscillation appears and the observed value of Γ is accumulated at $\Gamma \simeq 0.6$. Without a statistical deviations from the average, we have a clear boundary at $S_0 = S_1$; no limit cycle is excited in the region $S_0 < S_1$.

Let us examine the effect of statistical variance. We first study the statistical variance in the influx S, ε_f. The Gaussian statistics is assumed, and the amplitude of deviation $\overline{\varepsilon_f} = \sqrt{\left(S(t) - S_0\right)^2} = 0.05$ is applied to the case of $S_0 = 0.6$. There appear irregular ELMs as is shown in Fig.2. The distribution function is shown in Fig.2(b), which exhibits the finite probability of the transition, even below the critical value S_1. The resultant oscillation contains random component, so that we evaluate the averaged frequency of oscillations, $\langle f \rangle$, and the standard deviation σ, $\sigma = \sqrt{\langle T^2 \rangle - \langle T \rangle^2} \,/\, \langle T \rangle$, where T is the observed interval of oscillations. In Fig.3, $\langle f \rangle$ and σ are plotted for $\overline{\varepsilon_f} = 0.05$ as a function of S_0. (The case in the absence of the noise $(\overline{\varepsilon_f} = 0)$ is also plotted, where $\langle f \rangle = 0$ for $S_0 < S_1$, and a sharp boundary of f is obtained at $S_0 = S_1$.) We observe the probabilistic excitation and that the transition occurs well below the critical value. As S_0 becomes small, the standard deviation σ becomes large and we find, in this case, an approximate relation $\sigma \propto \langle f \rangle^{-0.74}$.

The probabilistic nature is also caused by the other statistical property of turbulence. The same statement is made for the variation in the hysteresis curve. The statistical variance of a is taken into account with $\overline{\varepsilon_a} = \sqrt{\langle a(t)^2 \rangle - \langle a \rangle^2}$. The Gaussian statistics is also assumed for ε_a. The

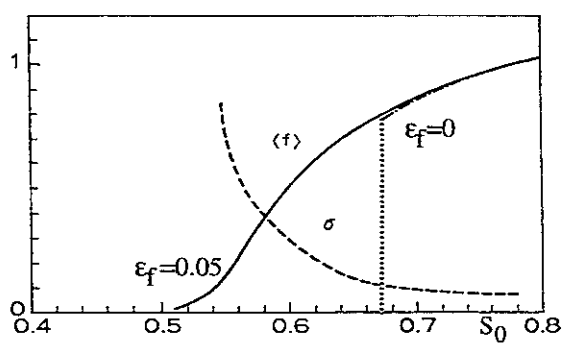

Fig.3 Average frequency and standard deviation of the bursts vs mean value of source S_0. In the absence of noise (dashed-dotted line), sharp discontinuity appears at $S_0 = S_1$.

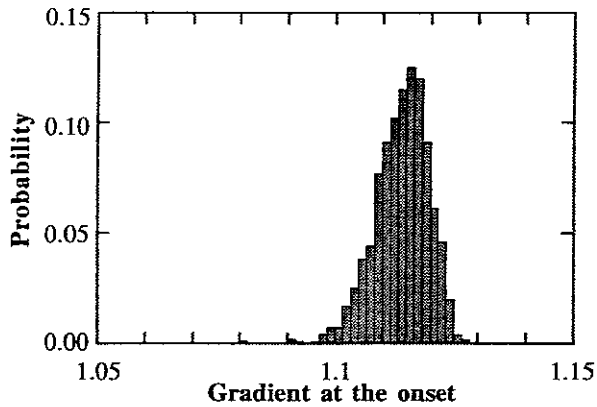

Fig.4 Distribution of the critical gradient at the onset of the crash. ($\overline{\varepsilon_a} = 0.05$). Statistical distribution of the critical gradient is observed.

finite probability of the onset of crash is observed for $S_0 < S_1$. Other quantities show similar results to those with finite ε_f.

To illustrate the probabilistic excitation of the transition, the observed critical pressure gradient for the onset of the crash is calculated. The limit cycle oscillation with irregular bursts are obtained for the case of $S_0 = 0.7$ and $\overline{\varepsilon_a} = 0.05$. The distribution function of α at the onset of crash is shown in Fig.4. The distribution clearly demonstrates that the onset becomes probabilistic in the presence of noise. If the deterministic picture is applied, the critical pressure at the onset converges to a particular value. ($\alpha_c = 1.13$)

IV. Summary and Discussion

In this paper, we show the probabilistic nature of the transition by a simple model equation. The model has features of the Langevin equation with the nonlinearlity of the Ginzburg-Landau model. The probability of the transition in the presence of fluctuations can be calculated in the presence of the statistical variance of relevant parameters. A probabilistic view of the crash rather than the deterministic view is proposed. The crash occurs, with finite probability, below the threshold condition of the deterministic picture. If the crash is heavily damaging, the concept of the life-time is naturally introduced.

We choose a Gaussian statistics for the deviations. Such a statistics has been applied to the thermal fluctuation near the thermal equilibrium, in which the excitation probability like the Arrhenius's law has been obtained. For the plasmas, the statistics of the deviation can be different from Gaussian statistics. The power law has been suggested from a simulation. The statistical study on the experiments of collapses will provide a unique information for the understanding of the physics of crash as well as the nature of the turbulence in plasmas.

Acknowledgements

This work is partly supported by the Grant-in-Aid for Scientific Research of Ministry of Education, Science, Sports and Culture, by JSPS Research Fellowships for Young Scientists and by collaboration programme of Advanced Fusion Research Center of Kyushu University.

References

[1] See a review, and papers there in: Itoh S-I et al. 1997, Physics of collapse events in toroidal plasmas, submitted to *Plasma Phys. Contr. Fusion*

[2] Itoh S-I et al. 1996 *Phys. Rev. Lett.* **76** 920.

[3] Fukuyama A et al. 1996 "Model of collapse of internal transport barrier", to be submitted.

[4] Lichtenberg A J et al. 1992 *Nucl. Fusion* **32** 495.

[5] Itoh K et al. 1995 *Plasma Phys. Contr. Fusion* **37** 707.

[6] Itoh S-I et al. 1991 *Phys. Rev. Lett.* **67** 2485.; ---- 1991 Research Report NIFS-96

[7] See a review and papers there in:
Itoh K and Itoh S-I 1996 *Plasma Phys. Contr. Fusion* **38** 1
Connor J W 1997 *Review of Models of ELMs*, this issue.

[8] Itoh S-I et al. 1993 *Nucl. Fusion* **33** 1445.

[9] Yagi M et al 1995 *Phys. Plasmas* **2** 4140.
---- 1997 *Chaos* **7** 198

[10] Endler M et al. 1995 *Nucl. Fusion* **35** 1307.

Recent Issues of NIFS Series

NIFS-469 V.L. Vdovin, T.Watari and A. Fukuyama,
3D Maxwell-Vlasov Boundary Value Problem Solution in Stellarator Geometry in Ion Cyclotron Frequency Range (final report); Dec. 1996

NIFS-470 N. Nakajima, M. Yokoyama, M. Okamoto and J. Nührenberg,
Optimization of M=2 Stellarator; Dec. 1996

NIFS-471 A. Fujisawa, H. Iguchi, S. Lee and Y. Hamada,
Effects of Horizontal Injection Angle Displacements on Energy Measurements with Parallel Plate Energy Analyzer; Dec. 1996

NIFS-472 R. Kanno, N. Nakajima, H. Sugama, M. Okamoto and Y. Ogawa,
Effects of Finite-β and Radial Electric Fields on Neoclassical Transport in the Large Helical Device; Jan. 1997

NIFS-473 S. Murakami, N. Nakajima, U. Gasparino and M. Okamoto,
Simulation Study of Radial Electric Field in CHS and LHD; Jan. 1997

NIFS-474 K. Ohkubo, S. Kubo, H. Idei, M. Sato, T. Shimozuma and Y. Takita,
Coupling of Tilting Gaussian Beam with Hybrid Mode in the Corrugated Waveguide; Jan. 1997

NIFS-475 A. Fujisawa, H. Iguchi, S. Lee and Y. Hamada,
Consideration of Fluctuation in Secondary Beam Intensity of Heavy Ion Beam Prove Measurements; Jan. 1997

NIFS-476 Y. Takeiri, M. Osakabe, Y. Oka, K. Tsumori, O. Kaneko, T. Takanashi, E. Asano, T. Kawamoto, R. Akiyama and T. Kuroda,
Long-pulse Operation of a Cesium-Seeded High-Current Large Negative Ion Source; Jan. 1997

NIFS-477 H. Kuramoto, K. Toi, N. Haraki, K. Sato, J. Xu, A. Ejiri, K. Narihara, T. Seki, S. Ohdachi, K. Adati, R. Akiyama, Y. Hamada, S. Hirokura, K. Kawahata and M. Kojima,
Study of Toroidal Current Penetration during Current Ramp in JIPP T-IIU with Fast Response Zeeman Polarimeter; Jan., 1997

NIFS-478 H. Sugama and W. Horton,
Neoclassical Electron and Ion Transport in Toroidally Rotating Plasmas; Jan. 1997

NIFS-479 V.L. Vdovin and I.V. Kamenskij,
3D Electromagnetic Theory of ICRF Multi Port Multi Loop Antenna; Jan. 1997

NIFS-480 W.X. Wang, M. Okamoto. N. Nakajima, S Murakami and N. Ohyabu,
Cooling Effect of Secondary Electrons in the High Temperature Divertor Operation; Feb. 1997

NIFS-481 K. Itoh, S.-I. Itoh, H. Soltwisch and H.R. Koslowski,
Generation of Toroidal Current Sheet at Sawtooth Crash; Feb. 1997

NIFS-482 K. Ichiguchi,
Collisionality Dependence of Mercier Stability in LHD Equilibria with Bootstrap Currents; Feb. 1997

NIFS-483 S. Fujiwara and T. Sato,
Molecular Dynamics Simulations of Structural Formation of a Single Polymer Chain: Bond-orientational Order and Conformational Defects; Feb. 1997

NIFS-484 T. Ohkawa,
Reduction of Turbulence by Sheared Toroidal Flow on a Flux Surface; Feb. 1997

NIFS-485 K. Narihara, K. Toi, Y. Hamada, K. Yamauchi, K. Adachi, I. Yamada, K. N. Sato, K. Kawahata, A. Nishizawa, S. Ohdachi, K. Sato, T. Seki, T. Watari, J. Xu, A. Ejiri, S. Hirokura, K. Ida, Y. Kawasumi, M. Kojima, H. Sakakita, T. Ido, K. Kitachi, J. Koog and H. Kuramoto,
Observation of Dusts by Laser Scattering Method in theJIPPT-IIU Tokamak Mar. 1997

NIFS-486 S. Bazdenkov, T. Sato and The Complexity Simulation Group,
Topological Transformations in Isolated Straight Magnetic Flux Tube; Mar. 1997

NIFS-487 M. Okamoto,
Configuration Studies of LHD Plasmas; Mar. 1997

NIFS-488 A. Fujisawa, H. Iguchi, H. Sanuki, K. Itoh, S. Lee, Y. Hamada, S. Kubo, H. Idei, R. Akiyama, K. Tanaka, T. Minami, K. Ida, S. Nishimura, S. Morita, M. Kojima, S. Hidekuma, S.-I. Itoh, C. Takahashi, N. Inoue, H. Suzuki, S. Okamura and K. Matsuoka,
Dynamic Behavior of Potential in the Plasma Core of the CHS Heliotron/Torsatron; Apr. 1997

NIFS-489 T. Ohkawa,
Pfirsch - Schlüter Diffusion with Anisotropic and Nonuniform Superthermal Ion Pressure; Apr. 1997

NIFS-490 S. Ishiguro and The Complexity Simulation Group,
Formation of Wave-front Pattern Accompanied by Current-driven Electrostatic Ion-cyclotron Instabilities; Apr. 1997

NIFS-491 A. Ejiri, K. Shinohara and K. Kawahata,
An Algorithm to Remove Fringe Jumps and its Application to Microwave Reflectometry; Apr. 1997

NIFS-492 K. Ichiguchi, N. Nakajima, M. Okamoto,

Bootstrap Current in the Large Helical Device with Unbalanced Helical Coil Currents; Apr. 1997

NIFS-493 S. Ishiguro, T. Sato, H. Takamaru and The Complexity Simulation Group,
V-shaped dc Potential Structure Caused by Current-driven Electrostatic Ion-cyclotron Instability; May 1997

NIFS-494 K. Nishimura, R. Horiuchi, T. Sato,
Tilt Stabilization by Energetic Ions Crossing Magnetic Separatrix in Field-Reversed Configuration; June 1997

NIFS-495 T. -H. Watanabe and T. Sato,
Magnetohydrodynamic Approach to the Feedback Instability; July 1997

NIFS-496 K. Itoh, T. Ohkawa, S. -I.Itoh, M. Yagi and A. Fukuyama
Suppression of Plasma Turbulence by Asymmetric Superthermal Ions; July 1997

NIFS-497 T. Takahashi, Y. Tomita, H. Momota and Nikita V. Shabrov,
Collisionless Pitch Angle Scattering of Plasma Ions at the Edge Region of an FRC; July 1997

NIFS-498 M. Tanaka, A.Yu Grosberg, V.S. Pande and T. Tanaka,
Molecular Dynamics and Structure Organization in Strongly-Coupled Chain of Charged Particles; July 1997

NIFS-499 S. Goto and S. Kida,
Direct-interaction Approximation and Reynolds-number Reversed Expansion for a Dynamical System; July 1997

NIFS-500 K. Tsuzuki, N. Inoue, A. Sagara, N. Noda, O. Motojima, T. Mochizuki, T. Hino and T. Yamashina,
Dynamic Behavior of Hydrogen Atoms with a Boronized Wall; July 1997

NIFS-501 I. Viniar and S. Sudo,
Multibarrel Repetitive Injector with a Porous Pellet Formation Unit; July 1997

NIFS-502 V. Vdovin, T. Watari and A. Fukuyama,
An Option of ICRF Ion Heating Scenario in Large Helical Device; July 1997

NIFS-503 E. Segre and S. Kida,
Late States of Incompressible 2D Decaying Vorticity Fields; Aug. 1997

NIFS-504 S. Fujiwara and T. Sato,
Molecular Dynamics Simulation of Structural Formation of Short Polymer Chains; Aug. 1997

NIFS-505 S. Bazdenkov and T. Sato
Low-Dimensional Model of Resistive Interchange Convection in Magnetized Plasmas; Sep. 1997

NIFS-506 H. Kitauchi and S. Kida,
Intensification of Magnetic Field by Concentrate-and-Stretch of Magnetic Flux Lines; Sep. 1997

NIFS-507 R.L. Dewar,
Reduced form of MHD Lagrangian for Ballooning Modes; Sep. 1997

NIFS-508 Y.-N. Nejoh,
Dynamics of the Dust Charging on Electrostatic Waves in a Dusty Plasma with Trapped Electrons; Sep.1997

NIFS-509 E. Matsunaga, T.Yabe and M. Tajima,
Baroclinic Vortex Generation by a Comet Shoemaker-Levy 9 Impact; Sep. 1997

NIFS-510 C.C. Hegna and N. Nakajima,
On the Stability of Mercier and Ballooning Modes in Stellarator Configurations; Oct. 1997

NIFS-511 K. Orito and T. Hatori,
Rotation and Oscillation of Nonlinear Dipole Vortex in the Drift-Unstable Plasma; Oct. 1997

NIFS-512 J. Uramoto,
Clear Detection of Negative Pionlike Particles from H_2 Gas Discharge in Magnetic Field; Oct. 1997

NIFS-513 T. Shimozuma, M. Sato, Y. Takita, S. Ito, S. Kubo, H. Idei, K. Ohkubo, T. Watari, T.S. Chu, K. Felch, P. Cahalan and C.M. Loring, Jr,
The First Preliminary Experiments on an 84 GHz Gyrotron with a Single-Stage Depressed Collector; Oct. 1997

NIFS-514 T. Shjmozuma, S. Morimoto, M. Sato, Y. Takita, S. Ito, S. Kubo, H. Idei, K. Ohkubo and T. Watari,
A Forced Gas-Cooled Single-Disk Window Using Silicon Nitride Composite for High Power CW Millimeter Waves; Oct. 1997

NIFS-515 K. Akaishi,
On the Solution of the Outgassing Equation for the Pump-down of an Unbaked Vacuum System; Oct. 1997

NIFS-516 *Papers Presented at the 6th H-mode Workshop (Seeon, Germany)*; Oct. 1997